ACS APPLIED MATERIALS & INTERFACES

Research Article

www.acsami.org

Graphene Quantum-Dot-Supported Platinum Nanoparticles: Defect-Mediated Electrocatalytic Activity in Oxygen Reduction

Yang Song and Shaowei Chen*

Department of Chemistry and Biochemistry, University of California, 1156 High Street, Santa Cruz, California 95064, United States

Supporting Information

ABSTRACT: Graphene quantum dot (GQD)-supported platinum (Pt/G) nanoparticles were prepared by a simple hydrothermal procedure at controlled temperatures. Transmission electron microscopic measurements showed that the platinum nanoparticles exhibited a rather consistent core size within the narrow range of 2.5−3.5 nm in diameter (average core diameters slightly lower than 3.0 nm) when the hydrothermal temperatures were varied between 140 and 180 °C, whereas at higher temperatures (200 °C) the nanoparticle core size was markedly larger, as a result of weakened anchoring and passivation of the metal nanoparticles by the diminishment of the GQD structural defects. Spectroscopic measurements based on Fourier-transformed infrared, Raman, and X-ray photoelectron spectroscopies confirmed the formation of various oxygenated structural defects on GQDs and the variation of their concentrations with the hydrothermal conditions. Interestingly, electrochemical studies showed that the electrocatalytic activity of the series exhibited a volcano-shaped variation with the GQD structural defects, with the best identified as the samples prepared at 160 °C for 12 h and at 180 °C for 6 h where the mass activity was found to meet the DOE target for 2017. This remarkable performance was accounted for by the deliberate manipulation of the adsorption of oxygen and reaction intermediates on platinum by the GQD structural defects through partial charge transfer. The strategy presented herein may offer a new paradigm in the design and engineering of nanoparticle catalysts for fuel cell electrochemistry.

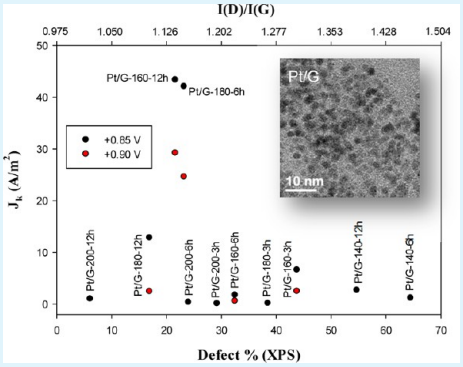

KEYWORDS: *graphene quantum dot, platinum nanoparticle, oxygen reduction, structural defect, Raman, XPS*

INTRODUCTION

In polymer exchange membrane fuel cells (PEMFCs),[1] both the oxidation of fuel molecules at the anode and reduction of oxygen at the cathode necessitate the use of effective catalysts so that sufficiently high current density is generated for practical applications. Of these, oxygen reduction reactions (ORRs) have long been recognized as a bottleneck that largely limits the fuel cell performance because of the complex reaction mechanism and sluggish electron-transfer kinetics. Platinum-based nanoparticles have been used extensively as the catalysts of choice for ORR.[2−8] These catalysts are generally dispersed onto supporting substrates with high specific surface areas and/or good electrical conductivity such as carbon black, carbon nanotubes, zeolite, tungsten carbides, Magneli phases of titanium oxides and indium tin oxides.[9−15] In the resulting composite structures, the substrates are generally thought to help stabilize the nanoparticles and improve the durability of the nanoparticle catalysts. Additionally, studies have shown that the electronic interactions between the metal nanoparticles and the supporting substrates may also play a significant role in determining the electrocatalytic activity as a result of the manipulation of the electronic energy of the metal nanoparticles and hence the interactions with oxygen.[16−19]

Recently, graphene derivatives have been attracting particular interest as a new functional support in fuel cell electrocatalysis,[20−23] due to their low cost, high surface area, high conductivity, and high chemical inertness that may facilitate electron-transfer reactions at the electrode surface and hence improve catalyst stability and durability.[24−27] In these studies, graphene sheets are generally produced from bulk graphite by the Hummers method through chemical oxidation and exfoliation with strong acids and oxidizing reagents.[28] Therefore, the graphene surface is decorated with various oxygen-containing functional groups (the products are hence commonly referred to as graphene oxide). Whereas the oxygen-containing groups on graphene oxide have been proposed to enhance Pt−support interactions, stabilize the nanoparticle catalysts, and prevent $\pi-\pi$ stacking between the graphene sheets, it has been claimed that the higher the graphitization degree of the carbon supports, the higher the electrochemical stability for carbon supported Pt catalysts.[27,29] Thus, the oxygenated species are generally removed from the graphitic structures so as to restore the sp^2 hybridized graphitic network for enhanced conductivity and stability of the graphene structures by chemical reduction and/or thermal treatment.[30,31]

Yet, in recent studies based on DFT calculations[32] and experiments,[33] it was proposed that structural defects of

Received: May 29, 2014
Accepted: July 14, 2014
Published: July 14, 2014

   dx.doi.org/10.1021/am503388z | ACS Appl. Mater. Interfaces 2014, 6, 14050−14060

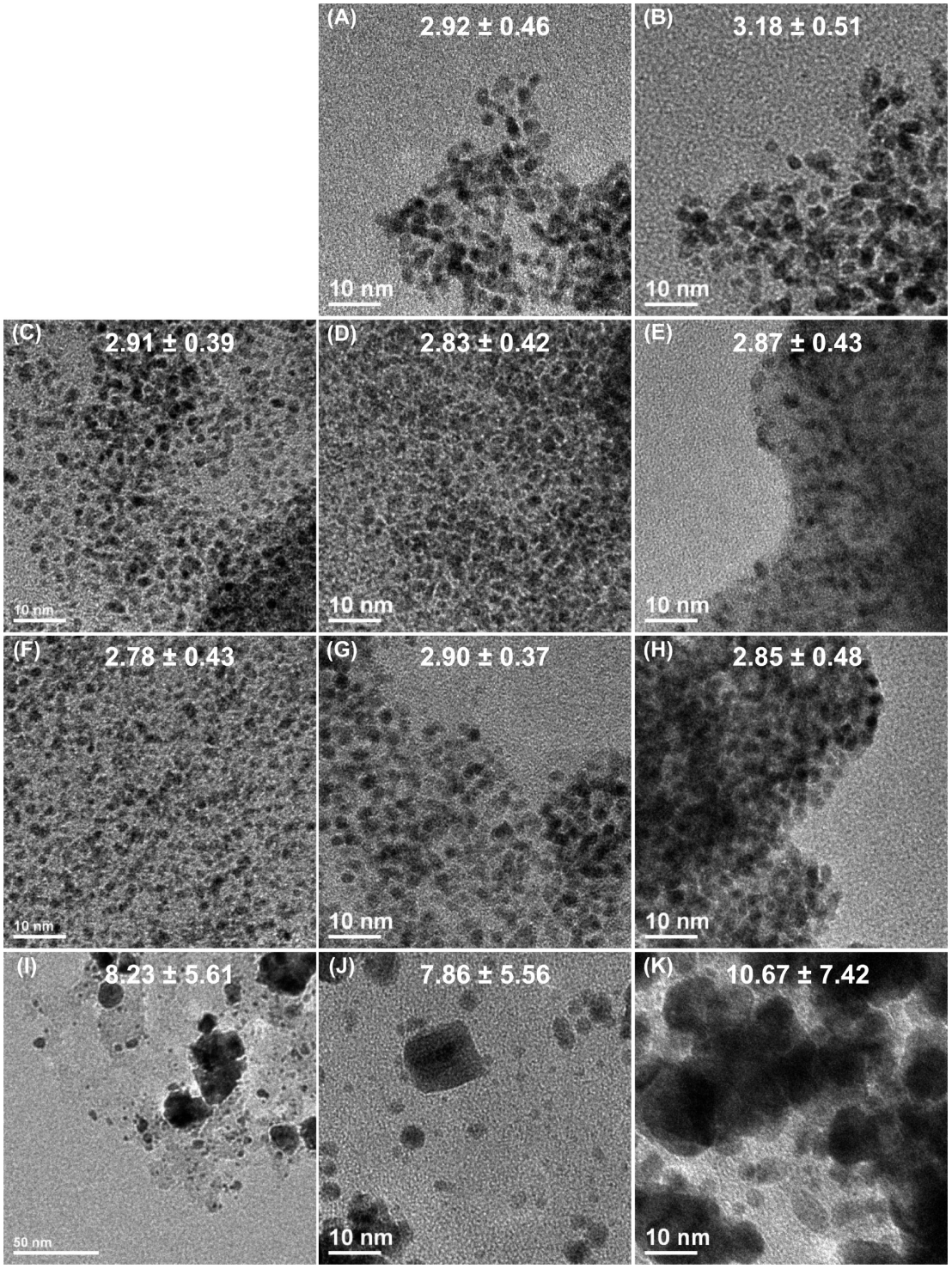

Figure 1. Representative TEM micrographs of GQD-supported Pt nanoparticles prepared by hydrothermal treatment at various temperatures for different periods of time: (A) 140 °C, 6 h; (B) 140 °C, 12 h; (C) 160 °C, 3 h; (D) 160 °C, 6 h; (E) 160 °C, 12 h; (F) 180 °C, 3 h; (G) 180 °C, 6 h; (H) 180 °C, 12 h; (I) 200 °C, 3 h; (J) 200 °C, 6 h; and (K) 200 °C, 12 h. Scale bars are all 10 nm except for panel (I) where it is 50 nm.

graphene might be exploited to promote charge transfer from platinum to oxygen as well as to manipulate the binding of reaction intermediates on the Pt surface, leading to enhancement of the ORR activity. In fact, we demonstrated experimentally[34] that platinum nanoparticles supported on graphene quantum dots (GQDs) indeed exhibited a markedly enhanced electrocatalytic performance with a more positive onset potential, higher specific activity as well as stability, as compared to commercial Pt/C, which was ascribed to the intimate electronic interactions between Pt nanoparticles and nanosized GQDs that manipulated the dissociative adsorption of oxygen and the binding of reaction intermediates on the Pt surface. Therefore, one immediate question arises. Is there an optimal concentration of structural defects within the GQDs that leads to maximal electrocatalytic activity of the Pt-GQD

Table 1. Summary of the Structures and Properties of Pt/G Nanoparticles Prepared at Different Hydrothermal Temperatures for Varied Periods of Time[a]

	d (nm)	I(D)/I(G)	x_d (%)	ECSA (m^2/g_{Pt})	onset potential (V)	J_k (A/m^2 at +0.90 V)
140 °C, 6 h	2.92 ± 0.46	1.49	64.6	14.91	0.87	
140 °C, 12 h	3.18 ± 0.51	1.26	54.7	16.25	0.96	
160 °C, 3 h	2.91 ± 0.39	1.35	43.8	19.16	0.96	2.48
160 °C, 6 h	2.83 ± 0.42	1.27	32.5	18.34	0.96	0.60
160 °C, 12 h	2.87 ± 0.43	1.20	21.6	30.87	1.02	29.2
180 °C, 3 h	2.78 ± 0.43	1.32	38.5	33.51	0.91	
180 °C, 6 h	2.90 ± 0.37	1.21	23.2	27.29	1.03	24.6
180 °C, 12 h	2.85 ± 0.48	1.17	16.9	33.56	0.96	2.43
200 °C, 3 h	8.23 ± 5.61	1.16	29.2	15.83	0.80	
200 °C, 6 h	7.86 ± 5.56	1.05	24.0	14.60	0.83	
200 °C, 12 h	10.67 ± 7.42	0.93	6.1	11.75	0.86	

[a]Average diameters (d, nm), I(D)/I(G) ratio from Raman measurements, fraction of defective carbon (x_d, %) from XPS measurements, effective electrochemical surface area (ECSA, m^2/g_{Pt}), onset potential (V), and kinetic current density (J_k, A/m^2) at +0.90 V.

nanocomposites for ORR? This is the primary motivation of the present work.

Note that the structural defects of GQDs may be manipulated by rather simple chemical processes. For instance, we have shown that hydrothermal treatment may be used to remove oxygen-contained groups on carbon nanoparticle surfaces in a controllable fashion, which is manifested by the enhancement of the nanoparticle photoluminescence as a result of the removal of surface trap states through dehydration and decarboxylation processes.[35] A similar hydrothermal procedure was also used in the conversion of graphene oxide to stable graphene suspension in water.[36,37] In these closed systems of relatively high temperatures and internal pressures, the degree of π-conjugation and hence the concentration of structural defects may be readily engineered by a deliberate control of the heating temperature and reaction time.

Therefore, in the present study, we adopted a literature procedure to prepare GQDs from carbon fibers, where the stacked submicrometer domains of traditional pitch-based carbon fibers were broken down to nanosized GQDs (1−4 nm with 1−3 layers in thickness) by acid treatments and chemical exfoliation.[38] Then, GQDs were used as supporting substrates for platinum nanoparticles by hydrothermal coreduction of GQDs and platinum precursors. The defect concentrations in GQDs were controlled by varying the heating temperature and reaction time of hydrothermal treatment and quantified by Raman and X-ray photoelectron spectroscopic (XPS) measurements. The electrocatalytic activity of the resulting nanocomposites (Pt/G) in oxygen reduction was then examined and compared in acid electrolyte solutions. Voltammetric measurements showed that while oxygen was effectively reduced to water at all nanoparticle catalysts, the electrocatalytic performance of the Pt/G nanocomposites exhibited volcano-shaped dependence on the defect concentration of the hydrothermally treated GQDs. The results were accounted for by the manipulation of the electronic interactions between the Pt nanoparticles and the nanosized GQDs through the GQD defects and their impacts on the adsorption of oxygen and reaction intermediates.

EXPERIMENTAL SECTION

Chemicals. Platinum(II) chloride ($PtCl_2$, 98%, Sigma-Aldrich), pitch carbon fibers (Fiber Glast Development Corporation), sodium carbonate (Na_2CO_3, ≥99.5%, Sigma-Aldrich), perchloric acid ($HClO_4$, 70 wt %, ACROS), sulfuric acid (H_2SO_4, Fisher Scientific), nitric acid (HNO_3, Fisher Scientific), and ultrahigh-purity oxygen (99.993%, Airgas) were used as received. Water was supplied via a Barnstead Nanopure water system (18.3 MΩ·cm).

Graphene Quantum Dots (GQDs). GQDs were prepared by following a literature procedure.[38] In brief, 1.00 g of carbon fibers was added into a mixture of concentrated H_2SO_4 (60 mL) and HNO_3 (20 mL). The solution was sonicated for 2 h and stirred for 24 h at 120 °C. The mixture was then cooled and diluted with Nanopure water (800 mL) with the pH adjusted to about 8 with Na_2CO_3. The solution was then dialyzed in a dialysis bag (cutoff molecular weight 2000 Da) for 3 days, affording purified GQDs. Atomic force microscopy (AFM) topographic studies showed that the thickness of the GQDs was 0.8−1.2 nm, corresponding to 2−3 graphene layers (Figure S1, Supporting Information). These GQDs were then used as supporting substrates for platinum nanoparticles, as detailed below.

GQD-Supported Platinum Nanoparticles (Pt/G). The procedure has been detailed previously.[34,38] In a typical reaction, $PtCl_2$ (6.65 mg, 0.025 mmol) was dissolved in 1 mL of hydrochloric acid under heating. The solution was then added into a 15 mL aqueous solution with 20 mg of GQDs prepared above under magnetic stirring (corresponding to a Pt loading of 20 wt %, same as that of commercial Pt/C catalysts). The pH was adjusted to 10 with NaOH, and the mixture was transferred to Teflon-lined autoclave and hydrothermally treated at 140, 160, 180, or 200 °C for 3, 6, or 12 h. Black precipitates appeared in the flask as a result of thermolytic reduction of Pt(II) and GQDs to form GQD-supported platinum nanoparticles. The precipitates were collected, washed extensively with Nanopure water and ethanol, and dried in a vacuum oven at room temperature for 12 h. The resulting nanoparticles were denoted as Pt/G-temperature-time. For instance, Pt/G-160-6h referred to the sample prepared at 160 °C for 6 h.

Structural Characterizations. High-resolution transmission electron microscopic (TEM) studies were carried out with a Philips CM200/FEG transmission electron microscope operated at 200 kV. Fourier transform infrared (FTIR) measurements were carried out with a PerkinElmer FTIR spectrometer (Spectrum One) where the samples were prepared by compressing the materials of interest into a KBr pellet. The spectral resolution was 4 cm^{-1}. Raman spectra were acquired with a DeltaNu Advantage 532 Raman system powered by a 532 nm laser. X-ray photoelectron spectra (XPS) were recorded with a PHI5400 instrument equipped with an Al Kα source operated at 350 W and at 10^{-9} Torr. The spectra were charge referenced to the Si 2p peak (99.3 eV) of a silicon substrate.

Electrochemistry. Electrochemical measurements were carried out with a CHI 440 electrochemical workstation using a standard three-electrode cell with separate anode and cathode compartments. A platinum foil and a reversible hydrogen electrode (RHE) were used as the counter and reference electrode, respectively. The working electrode was a glassy-carbon disk electrode (diameter 5.61 mm) of a rotating ring-disk electrode (RRDE, with a collection efficiency of

37%) from Pine Instrument.[39] The RRDE electrode was prepared according to a procedure described by Gloaguen et al.[40] In a typical experiment, a calculated amount of Pt/G nanocomposites was mixed under ultrasound with a Nafion solution (5 wt %, Fluka) to form a well-dispersed catalyst ink. The catalyst ink was then drop-cast onto the polished glassy-carbon disk electrode at a mass loading of the Pt/G nanocpmposites of 27.5 μg, corresponding to a Pt loading of ca. 3 μg, as determined by XPS measurements (vide infra). Prior to electrochemical tests of oxygen reduction, the catalyst films on the glassy-carbon electrode surface were electrochemically pretreated in a nitrogen-saturated 0.1 M $HClO_4$ solution by rapid potential cycling at 200 mV/s between +0.05 and +1.10 V until a steady voltammogram was observed. The electrocatalytic activity for oxygen reduction was then evaluated in an O_2-saturated 0.1 M $HClO_4$ solution. The solution ohmic drop (i.e., IR drop) was electronically compensated.

RESULTS AND DISCUSSION

Figure 1 shows the representative TEM images of the Pt/G nanoparticles prepared at various temperatures for different periods of time. It can be seen that the dark-contrast objects are platinum nanoparticles which are dispersed rather homogeneously on the graphene surface that appears as a low-contrast background. Statistical analysis based on more than 200 nanoparticles in each sample, as manifested in the core size histograms in Figure S2, shows that the majority of the Pt nanoparticles are in the narrow range of 2.5−3.5 nm in diameter (with the averages slightly less than 3.0 nm) when the hydrothermal temperatures were kept within the range of 140−180 °C, and at the higher temperature of 200 °C the nanoparticles are markedly larger at 8−12 nm in diameter. Such a discrepancy of the nanoparticle core size (Table 1) might be ascribed to the variation of the concentration of GQD structural defects which can be deliberately controlled by hydrothermal conditions. Note that the GQD structural defects likely serve as the anchoring sites for platinum precursors and the growth of platinum nanoparticles.[41] At high hydrothermal temperatures, the diminishment of the concentration of the structural defects renders it difficult to effectively passivate the Pt nanoparticles, hence leading to a marked increase of the particle size.[42] Furthermore, in high-resolution TEM studies (Figure S3), clearly defined lattice fringes can be identified, with a spacing of 0.236 nm. These are consistent with the (111) crystalline planes of fcc Pt.[39]

The formation of Pt-GQD nanocomposites was manifested in FTIR measurements. Figure 2 depicts the FTIR spectra of the as-prepared GQDs and Pt/G composites prepared under various hydrothermal conditions. All samples exhibit one broad peak at about 3430 cm^{-1}, which is attributed to the hydroxyl groups of the GQDs (and residual water).[43] For the as-prepared GQDs (black curve), several strong peaks can also be identified at 1685 cm^{-1} (C═O carboxyl or carbonyl stretching vibrations), 1350 cm^{-1} (O−H deformation in the C−OH group), and 1135 cm^{-1} (C−O−C asymmetric stretching vibration in epoxide), suggesting the presence of various oxygenated species on the GQD surfaces. In addition, two strong vibrational bands can be seen at 1606 and 1443 cm^{-1} which were attributed to the C═C stretching vibration of unoxidized graphitic (sp^2) domains.[44] Almost identical vibrational features can be seen with the Pt/G-140-6h sample (red curve), signifying that hydrothermal treatment under this condition did not lead to a marked change of the GQD structures.

For other Pt/G hybrid nanoparticles, however, apparent differences can be seen. First, the O−H vibrations diminished

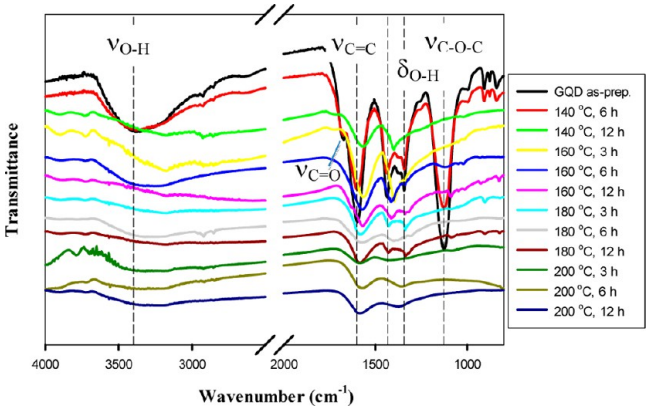

Figure 2. FTIR spectra of Pt/G nanoparticles prepared by hydrothermal treatments at different temperatures for various periods of time (specified in figure legend). The spectrum for the as-prepared GQDs is also included as the black curve.

markedly, and the C═O and C−O−C stretches almost disappeared, signifying effective removals of these functional moieties from the GQD surfaces. Second, the C═C stretches exhibited an apparent red-shift to 1593 and 1410 cm^{-1} (Pt/G-140-12h, green curve), 1583 and 1405 cm^{-1} (Pt/G-160-3h, yellow curve), 1593 and 1429 cm^{-1} (Pt/G-160-6h, blue curve), 1587 and 1431 cm^{-1} (Pt/G-160-12h, magenta curve). This may be accounted for by the restoration and hence growth of the Csp^2 domains in GQDs. With a further increase of the hydrothermal temperature the change was minimal, as the C═C stretches now appeared at 1602 and 1436 cm^{-1} for Pt/G-180-3h (aqua blue curve), 1602 and 1431 cm^{-1} for Pt/G-180-6h (gray curve), 1603 and 1441 cm^{-1} for Pt/G-180-12h (brown curve), 1606 and 1455 cm^{-1} for Pt/G-200-3h (dark green curve). For the Pt/G-200-6h (chartreuse curve) and Pt/G-200-12h (dark blue curve) samples, the C═C stretches can be found at 1599 and 1356 cm^{-1}, consistent with the G and D bands observed in Raman spectroscopic measurements (Figure 3 below).

A more quantitative assessment of the GQD defects was then carried out by Raman spectroscopic measurements. From Figure 3, one can see that the series of Pt/G nanocomposites all

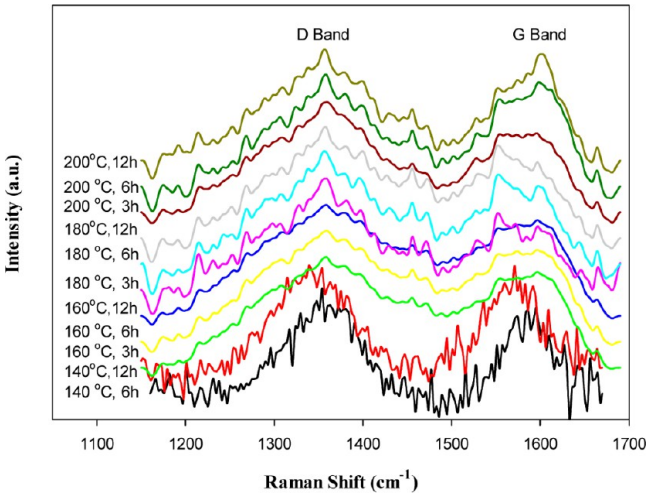

Figure 3. Raman spectra of Pt/G nanoparticles prepared by hydrothermal treatments at different temperatures for various periods of time (specified in figure legend).

exhibited two bands at ca. 1593 and 1352 cm^{-1}, corresponding to the G band and D band of graphitic nanostructures, respectively. Note that the G band is assigned to the E_{2g} phonon of the sp^2 carbons, while the D band is a breathing mode of the κ-point phonons of A_{1g} symmetry.[45,46] A prominent D band is an indication of structural disorder in the GQDs, originating from defects associated with vacancies, grain boundaries and amorphous carbon species, which has been observed extensively with chemical exfoliated graphene oxide;[47,48] and the ratio (I(D)/I(G)) of the D and G band intensity may be exploited for the quantitative assessment of the relative concentration of structural defects within the graphitic carbon matrix.[49] Table 1 lists the I(D)/I(G) values for the series of Pt/G hybrid nanoparticles prepared under different hydrothermal conditions. There are several aspects that warrant attention. First, for the same reaction time, increasing hydrothermal temperature led to a decrease of the I(D)/I(G) ratio. For instance, for 6 h of hydrothermal treatment, the I(D)/I(G) ratio for the samples prepared at 140 °C is 1.49, 1.27 at 160 °C, 1.21 at 180 °C, and 1.05 at 200 °C, indicating more effective removal of structural defects (and restoration of the Csp^2 domains) at higher temperature and growth of the Csp^2 domains. Additionally, at any given temperature, the I(D)/I(G) ratio also decreases with increasing reaction time. For instance, at the hydrothermal temperature of 160 °C, the I(D)/I(G) ratio decreased from 1.35 at 3 h to 1.27 at 6 h and 1.20 at 12 h. Same behaviors can be seen at other hydrothermal temperatures. Thus, within the present experimental context, the lowest I(D)/I(G) ratio was observed at 0.93 with the Pt/G nanocomposites prepared at 200 °C for 12 h. These observations confirm that the hydrothermal treatment is indeed an effective method in removing defects in carbon nanostructures and the defect density can be readily controlled by experimental conditions (temperature, reaction time, etc.), in good agreement with results of the FTIR measurements (Figure 2).[36,37]

Such a structural variation was also quantified by XPS measurements. Figure 4 depicts the survey spectra of the (A) C 1s and (B) Pt 4f electrons of the Pt/G nanocomposites prepared at different temperatures by hydrothermal treatment. In panel (A), for the Pt/G-140-6h sample, deconvolution of the C 1s electron spectra revealed four major components of the carbon 1s electrons: sp^2 carbon at 284.7 eV (yellow curve),[50−54] carbons in C−OH at 286.2 eV (blue curve),[55] in C═O at 287.4 eV (magenta curve), and in COOH at 289.9 eV (aqua blue curve) bonds.[38,56,57] This further confirms the formation of various oxygenated functional moieties on the GQD surfaces. If one defines all non-sp^2 carbon as the structural defects, one can see that whereas the binding energies remained virtually unchanged (Table S1), the defect concentration in the Pt/G nanocomposites decreased markedly with increasing hydrothermal temperature and prolonging reaction time, as manifested by the apparent diminishment of the non-sp^2 carbon peaks. In fact, from the top panel of Figure S4, one can see that (i) during the hydrothermal treatment, C═O and COOH defects were more readily removed, leaving C−O as the primary defects remaining in the GQDs (blue peaks); and (ii) the defect concentration reaches a minimum (~20%) and correspondingly the C sp^2 fraction reaches a maximum (~80%) at Pt/G-160-12h. These observations are consistent with the Raman spectroscopic results (Figure 3 and Table 1). In fact, the atomic ratio of defective carbons to total carbon exhibited a roughly linear increase with the I(D)/I(G) ratio, from 6.1% at

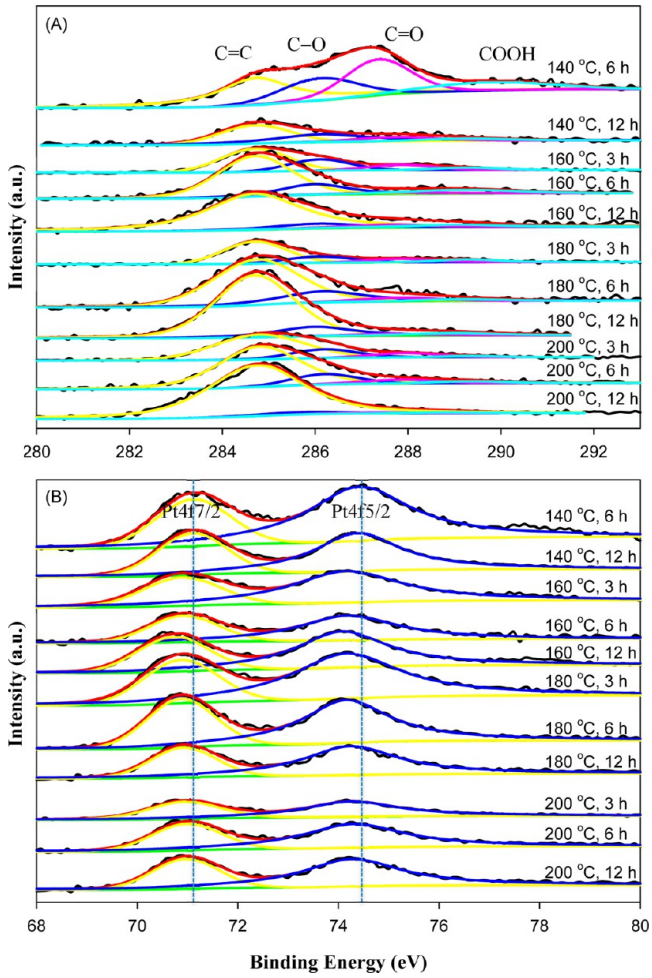

Figure 4. XPS spectra of (A) C 1s and (B) Pt 4f electrons of the Pt/G nanoparticles prepared by a hydrothermal procedure at different temperatures for various periods of time (specified in figure legend). Black curves are experimental data, and colored curves are deconvolution fits.

I(D)/I(G) = 0.93 to 64.8% at I(D)/I(G) = 1.49, as manifested in the bottom panel of Figure S4, suggesting a direct correlation between these two measurements.

From panel (B) of Figure 4, the binding energies of the Pt 4f electrons in the Pt/G nanocomposites can all identified at around 71.0 and 74.4 eV where both the doublet energies and spin−orbit coupling are consistent with those of metallic platinum (Table S1).[58,59] Interestingly, from Table S1, it can be seen that both binding energies of the Pt 4f electrons first decreased with increasing temperature from 140 to 180 °C, and then increased when the hydrothermal temperature increased to 200 °C. Specifically, the lowest binding energies for Pt $4f_{7/2}$ and Pt $4f_{5/2}$ among the series can be found at 70.9 and 74.2 eV for Pt/G-160-12h (and only slightly higher with Pt/G-180-6h). In contrast, the binding energies are the highest at 71.1 and 74.4 eV for both Pt/G-140-6h and Pt/G-200-12h. Interestingly, among the three major defects (C−OH, C═O, and COOH), the corresponding binding energy of the C 1s electrons in C═O was 287.7 eV for Pt/G-160-12h, but markedly lower at 287.4 eV for both Pt/G-140-6h and Pt/G-200-12h, whereas those for C−OH and COOH were virtually invariant. This discrepancy suggests that charge transfer likely occurred from Pt to GQD that was dictated largely by the polar carbonyl (C═O)

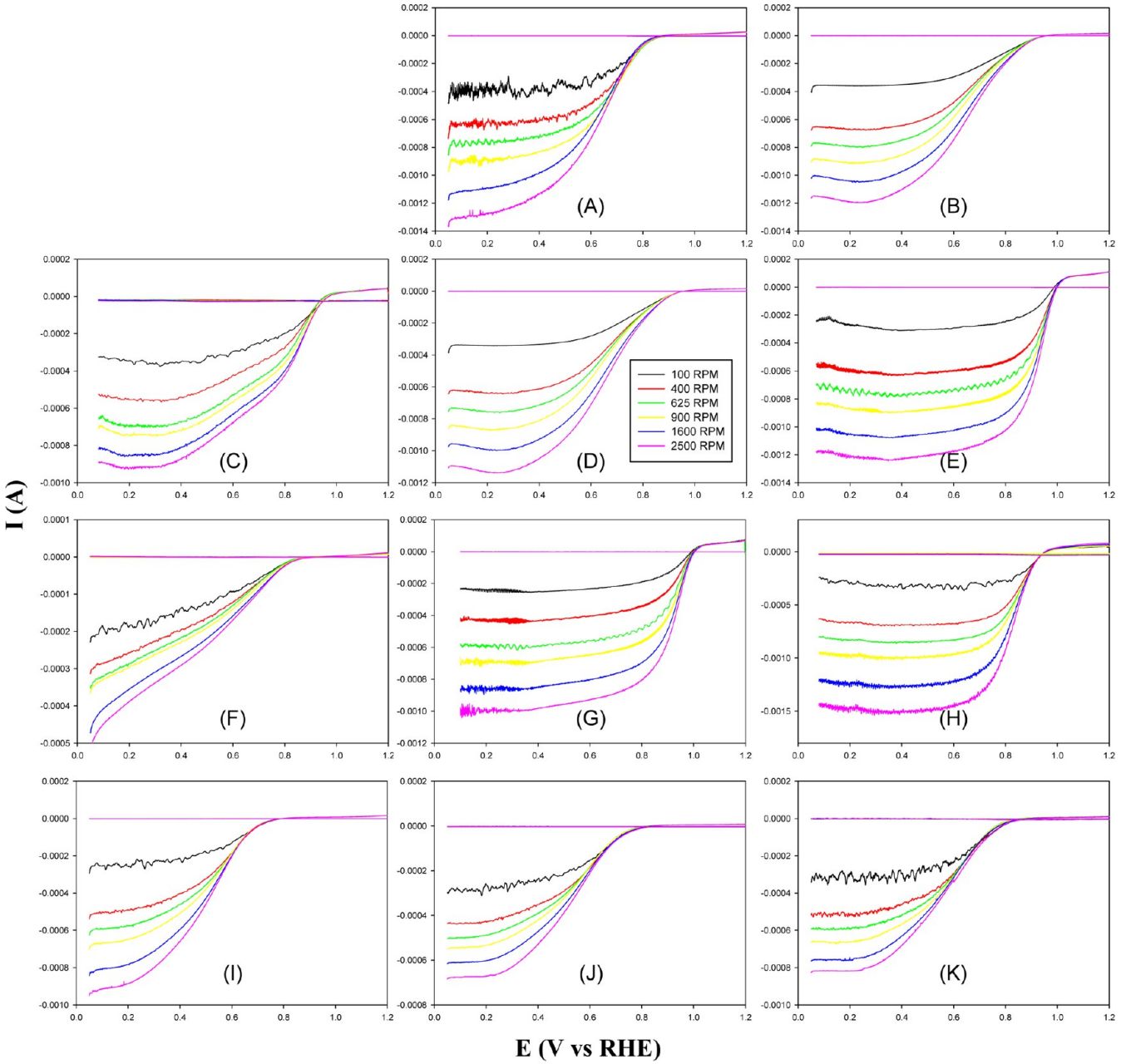

Figure 5. RRDE voltammograms of GQD-supported Pt nanoparticles prepared by hydrothermal treatment at different temperatures for various period of time: (A) 140 °C, 6 h; (B) 140 °C, 12 h; (C) 160 °C, 3 h; (D) 160 °C, 6 h; (E) 160 °C, 12 h; (F) 180 °C, 3 h; (G) 180 °C, 6 h; (H) 180 °C, 12 h; (I) 200 °C, 3 h; (J) 200 °C, 6 h; and (K) 200 °C, 12 h. Pt catalyst loadings were around 3 μg as listed in Table S3. Potential sweep rate is 5 mV/s, and electrode rotation rates are specified in the figure legend. Ring potentials were all set at +1.5 V.

moieties on the GQD surfaces, and this charge transfer reached a minimum in the Pt/G-160-12h and Pt/G-180-6h samples among the series, because of low concentrations of the polar C═O and COOH structural defects (Figure S4). Interestingly, electrochemical measurements indicate that these two samples exhibited the best electrocatalytic activities in ORR among the series, as detailed below.

Furthermore, from the integrated peak areas in the XPS measurements, the concentration of Pt in the Pt/G nanocomposites can be quantified. The results are summarized in Table S2, where one can see that the platinum loading (Pt/C atomic ratio) was quite consistent among the nanocomposite series at between 11% and 14%.

The electrocatalytic activity of the resulting Pt/G nanocomposites was then examined for oxygen reduction reactions. Figure S5 shows the steady-state cyclic voltammograms of a glassy carbon electrode modified with the same amount of Pt/G in a 0.1 M $HClO_4$ solution saturated with nitrogen. Note that the Pt mass loading was estimated by XPS measurements to be between 3.0 and 3.8 μg (Table S2). All samples exhibited the well-defined butterfly voltammetric features of platinum in nitrogen-saturated acid electrolytes. Of these, a pair of broad voltammetric peaks can be seen within the potential range of +0.3 and +0.7 V, which are ascribed to the formation of platinum oxide in the anodic scan and reduction of the oxide in the return sweep. Two additional pairs of voltammetric peaks appeared between 0 and −0.3 V. These are due to hydrogen

dx.doi.org/10.1021/am503388z | ACS Appl. Mater. Interfaces 2014, 6, 14050−14060

adsorption/desorption on the platinum surface. Based on the integrated areas of these voltammetric features, the effective electrochemical surface area (ECSA) of the nanoparticle catalysts were calculated to be between 11 and 33 m^2/g_{Pt}, depending on the nanoparticle size. The results are listed in Table 1.

The electrocatalytic activity in oxygen reduction was then examined by voltammetric measurements in an oxygen-saturated 0.1 M $HClO_4$ solution. Figure 5 shows the RRDE voltammograms of the glassy carbon disk electrode modified with Pt/G nanoparticles with the electrode rotation rate varied from 100 to 2500 rpm. There are at least two aspects that warrant attention here. First, nonzero cathodic currents at the disk electrode (I_D) became clearly identified as the electrode potential was swept in the negative direction, and the currents increased with increasing electrode rotation rates, signifying the apparent electrocatalytic activity of the Pt/G nanoparticles in oxygen reduction (one may see that nonzero anodic currents appeared at the disk electrode at very positive potentials for all samples, in particular for samples C, E, G, and H. The origin of this is unknown at the moment. Yet the marked difference of their ORR activity implies that it is unlikely that the ORR activity was impacted by this phenomenon). Second, the corresponding ring currents (I_R) at +1.5 V were about 3 orders of magnitude lower than those of the disk, signifying that only minimal amounts of peroxide intermediates were produced during oxygen reduction and hence high efficiency of the Pt/G nanoparticles in the electrocatalytic process. In fact, the number of electron transfer (n) during oxygen reduction can be estimated by the ratio between the disk and the ring currents,[39,60,61]

$$n = \frac{4I_D}{I_D + \frac{I_R}{N}} \tag{1}$$

where N is the collection efficiency (37%) of the RRDE electrode,[39] as depicted in Figure 6. It can be seen that at sufficiently negative potentials, all electrodes exhibited $n \approx 4.00$, indicating that oxygen was fully reduced into water, $O_2 + 4H^+ + 4e \rightarrow 2H_2O$. Yet the onset potential for oxygen reduction was markedly different, as listed in Table 1. Among the series, the onset potentials decreases in the order of Pt/G-180-6h (+1.03 V) > Pt/G-160-12h (+1.02 V) > Pt/G-180-12h ≈ Pt/G-160-6h ≈ Pt/G-160-3h ≈ Pt/G-140-12h (+0.96 V) > Pt/G-180-3h (+0.91 V) > Pt/G-140-6h (+0.87 V) > Pt/G-200-12h (+0.86 V) > Pt/G-200-6h (+0.83 V) > Pt/G-200-3h (+0.80 V). That is, Pt/G-180-6h and Pt/G-160-12h are among the best in the series with the most positive onset potential.

The electron-transfer kinetics involved were then quantified by the Koutecky–Levich analysis (eq 2), as the disk currents (I_D) might include both kinetic (I_k)- and diffusion (I_d)-controlled contributions,

$$\frac{1}{I_D} = \frac{1}{I_k} + \frac{1}{I_d} + \frac{1}{I_k} + \frac{1}{B\omega^{1/2}} \tag{2a}$$

$$B = 0.62nFAC_O D_O^{2/3} \nu^{-1/6} \tag{2b}$$

$$I_k = nAFkC_O \tag{2c}$$

where F is the Faradaic constant (96500 C/mol), D_O the diffusion coefficient of O_2 in 0.1 M $HClO_4$ aqueous solution (1.93×10^{-5} cm^2/s), ν the kinematic viscosity of the solution (9.87×10^{-3} cm^2/s), C_O the oxygen concentration in O_2-saturated solutions (1.18 mM), ω the electrode rotation rate, k the electron-transfer rate constant, and A the geometric surface area of the electrode.[62−64] Figure S6 depicts the Koutecky–Levich plots (I_D^{-1} vs $\omega^{-1/2}$) of all Pt/G nanoparticles within the respective kinetically controlled region. First, one can see that all experimental data exhibited good linearity, and the slopes were rather consistent with each nanoparticle sample. This indicates that the oxygen reduction proceeded at the Pt/G nanoparticle catalysts as a first-order reaction with respect to dissolved oxygen.

In addition, from the linear regressions in Figure S6, the kinetic currents (I_k) could also be quantified from the y-axis intercepts (eq 2c). This is manifested in the Tafel plot of Figure 7. It can be clearly seen that at all Pt/G nanoparticle catalysts the kinetic current densities increased with increasingly negative electrode potentials, and more importantly, within the electrode potential range of +0.80 to +1.00 V, the kinetic current densities with Pt/G-160-12h and Pt/G-180-6h were at least an order of magnitude higher than those of other Pt/G

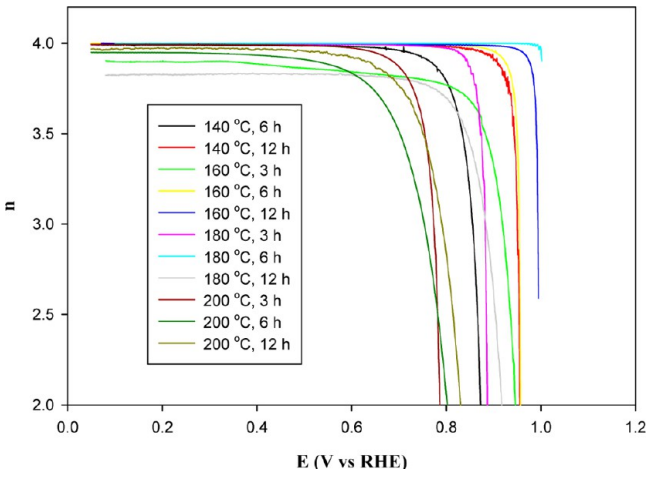

Figure 6. Variation of the number of electron transfer (n) in oxygen reduction with electrode potential. Curves are average values of experimental data calculated from the RRDE voltammograms at all rotation rates in Figure 5 by using eq 1.

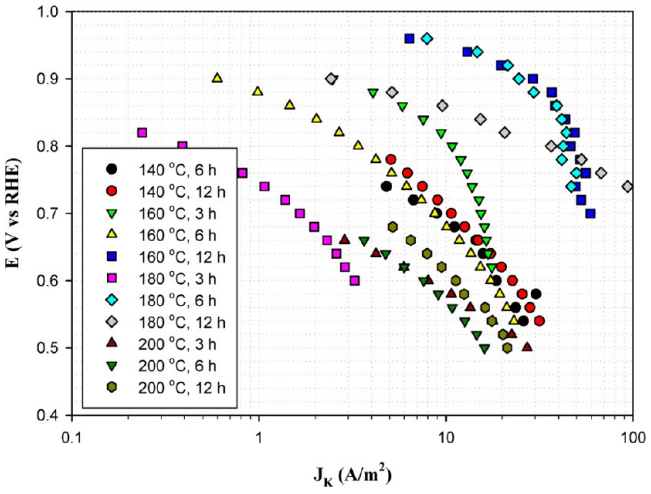

Figure 7. Tafel plot of the Pt/G nanoparticles for oxygen reduction. Symbols are experimental data obtained by linear regressions of the Koutecky–Levich plots (Figure S6) with eq 2.

samples. For instance, the area-specific current density (J_k, I_k normalized by the respective effective electrochemical surface area as determined in Figure S5, Table 1) at +0.90 V was 29.2 and 24.6 A/m^2 for these two catalysts, respectively, but only 2.48 A/m^2 for Pt/G-160-3h, 2.43 A/m^2 for Pt-180-12h, and 0.60 A/m^2 for Pt/G-160-6h (for the rest, the currents were too small to measure). These are significantly greater than that observed with Pt/G nanocomposites prepared without hydrothermal treatment (14.5 A/m^2), and more than an order of magnitude higher than that of commercial Pt/C.[34]

In terms of mass activity, the Pt/G-160-12h and Pt/G-180-6h samples also stood out as the best among the series at 468.1 and 435.7 A/g_{Pt} at +0.90 V, respectively. Note that these have reached the Department of Energy (DOE) target for 2017 (440 A/g_{Pt} at +0.90 V), and are also superior to commercial Pt/C catalysts (~160 A/g)[39,65,66] and leading Pt-based alloy catalysts reported so far, such as PtNi nanooctahedras (300−360 A/g),[66] PtPd nanodendrites (240 A/g),[67] PtAu (200−300 A/g),[68] and PtCuCoNi nanotubes (190 A/g).[69] In contrast, the mass activity was only 40.1 A/g_{Pt} for Pt/G-180-12h, 38.3 A/g_{Pt} for Pt/G-160-3h, and 9.4 A/g_{Pt} for Pt/G-160-6h.

This remarkable performance of the Pt/G nanocomposites for oxygen reduction might be accounted for by the impacts of the GQD structural defects on the reaction dynamics of ORR. In a recent study based on density functional theory calculations of a Pt_{13} nanoparticle supported on a monovacancy defective graphene nanosheet,[32] it was found that the defective graphene support not only lowered the activation energy for oxygen (O_2) dissociation by promoting charge transfer from Pt to O_2 but also decreased the energy barrier of the rate-limiting step by weakening the binding of the HO* species. Indeed, drastic enhancement was observed with GQD-supported Pt nanoparticles in ORR, in comparison to commercial Pt/C catalysts.[34] In the present study, the results presented above demonstrate that the performance may be further enhanced by a deliberate manipulation of the GQD structural defects, as shown in Figure 8. Using the kinetic current densities at +0.85 V (black circles) and +0.90 V (red circles) as the measuring yardsticks, we can see that the electrocatalytic activity of the Pt/G nanocomposites exhibited volcano-shaped dependence on the defect concentrations quantified by XPS measurements (Figure 4) and on the I(D)/I(G) ratio determined by Raman spectroscopic measurements (Figure 3), with the best activity in the series both corresponding to the Pt/G-160-12h and Pt/G-180-6h samples. This means that there exists an optimal defect concentration within the GQDs for maximal ORR activity of the Pt/G hybrid nanoparticles. This may be ascribed to the intimate interactions between the graphene support and platinum nanoparticles that led to deliberate manipulation of the platinum d-band center and hence the charge transfer dynamics of oxygen reduction.[32]

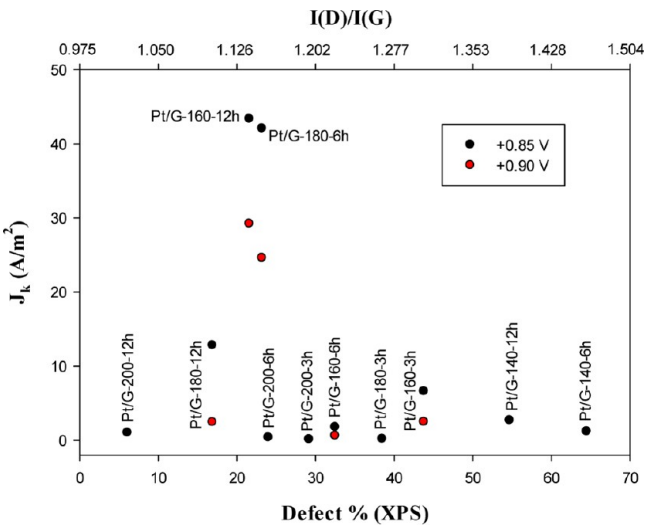

Figure 8. Variation of the ORR kinetic current density at +0.85 (solid circles) and +0.90 V (empty circles) with GQD structural defects manifested as the defect concentrations from XPS measurements (Figure 4) and I(D)/I(G) ratio in Raman spectroscopic measurements (Figure 3).

Mechanistically, in oxygen reduction, it has been known that the electron-transfer kinetics and hence the electrocatalytic performance depend rather sensitively on the adsorption of oxygen and reaction intermediates such as O* and HO* intermediates on the Pt surface. In fact, studies have shown that the optimal catalytic activity for ORR may be achieved when oxygen adsorption is 0.1 eV weaker than that on single-crystal platinum electrode surfaces.[70−72] Thus, ideally a balance has to be struck between the strength of intermediate adsorption and reaction kinetics. This may be achieved by a deliberate variation of the GQD structural defects as a result of partial charge transfer from platinum that weakens the adsorption of oxygen and reaction intermediates. In the present study, the experimental results suggest that an optimal structure may be found at about 20% defect concentration of the GQD supports. Whereas higher concentration of the GQD defects may afford more substantial charge transfer from Pt to GQD, the electronic conductivity of the GQDs support may suffer and hence compromise the electron transfer kinetics of oxygen reduction.

CONCLUSION

In this study, graphene quantum dot (GQD)-supported platinum nanoparticles were prepared by hydrothermal coreduction of Pt(II) precursors and GQDs within the temperature range of 140−200 °C for various periods of time. TEM measurements showed that the Pt nanoparticles exhibited rather consistent core size when the hydrothermal temperature was controlled between 140 and 180 °C, and at higher temperatures (200 °C) the particle core size was found to increase drastically, which was accounted for by the diminishment of the structural defects of the GQDs that weakened the anchoring and passivation of the platinum nanoparticles. Interestingly, the GQD structural defects, which were examined and quantified by FTIR, Raman, and XPS spectroscopic measurements, were found to strongly impact the electrocatalytic activity of the resulting Pt/G nanocomposites in oxygen reduction. On the basis of the onset potential, number of electron transfer involved, and kinetic current density, the Pt/G-160-12h and Pt/G-180-6h nanoparticles were found to exhibit markedly enhanced electrocatalytic activity as compared to the rest of the series, with the mass activity reaching the DOE target for 2017. This suggests an optimal defect concentration of about 20% of non-sp^2 carbons in GQDs as determined by XPS measurements, or an I(D)/I(G) ratio of about 1.2 in Raman spectroscopic measurements. The results are rationalized by the manipulation of the adsorption of oxygen and reaction intermediates on platinum by the GQD structural defects as partial charge transfer might occur from Pt to GQD defects. Additional contributions might arise from the

effects of structural defects on the electronic conductivity of the nanocomposites catalysts. The results presented herein are significant in that the strategy may lead to the development of a new paradigm in the design, manipulation, and optimization of nanoparticle catalysts for fuel cell electrochemistry.

■ ASSOCIATED CONTENT

Supporting Information

Representative AFM topograph of GQDs, high-resolution TEM micrographs, core size histograms, concentrations of structural defects of Pt/G nanocomposites by XPS and Raman measurements, additional cyclic voltammograms and Koutecky–Levich plots in ORR. This material is available free of charge via the Internet at http://pubs.acs.org

■ AUTHOR INFORMATION

Corresponding Author

*E-mail: shaowei@ucsc.edu.

Author Contributions

The manuscript was written through contributions of all authors. All authors have given approval to the final version of the manuscript.

Notes

The authors declare no competing financial interest.

■ ACKNOWLEDGMENTS

This work was supported, in part, by the National Science Foundation (CHE-1012258 and CHE-1265635). TEM and XPS studies were carried out at the National Center for Electron Microscopy and Molecular Foundry, Lawrence Berkeley National Laboratory as part of a user project.

■ REFERENCES

(1) Behling, N. H. *Fuel Cells: Current Technology Challenges and Future Research Needs*, 1st ed.; Elsevier: Boston, 2013.

(2) Gasteiger, H. A.; Kocha, S. S.; Sompalli, B.; Wagner, F. T. Activity Benchmarks and Requirements For Pt, Pt-Alloy, and non-Pt Oxygen Reduction Catalysts for PEMFCs. *Appl. Catal., B* **2005**, *56*, 9–35.

(3) Stamenkovic, V. R.; Fowler, B.; Mun, B. S.; Wang, G. F.; Ross, P. N.; Lucas, C. A.; Markovic, N. M. Improved Oxygen Reduction Activity on $Pt_3Ni(111)$ via Increased Surface Site Availability. *Science* **2007**, *315*, 493–497.

(4) Zhang, J.; Sasaki, K.; Sutter, E.; Adzic, R. R. Stabilization of Platinum Oxygen-Reduction Electrocatalysts Using Gold Clusters. *Science* **2007**, *315*, 220–222.

(5) Wang, C.; Markovic, N. M.; Stamenkovic, V. R. Advanced Platinum Alloy Electrocatalysts for the Oxygen Reduction Reaction. *ACS Catal.* **2012**, *2*, 891–898.

(6) Tian, N.; Zhou, Z.-Y.; Sun, S.-G.; Ding, Y.; Wang, Z. L. Synthesis of Tetrahexahedral Platinum Nanocrystals with High-Index Facets and High Electro-Oxidation Activity. *Science* **2007**, *316*, 732–735.

(7) Wang, D. L.; Xin, H. L. L.; Hovden, R.; Wang, H. S.; Yu, Y. C.; Muller, D. A.; DiSalvo, F. J.; Abruna, H. D. Structurally Ordered Intermetallic Platinum-Cobalt Core-Shell Nanoparticles with Enhanced Activity and Stability as Oxygen Reduction Electrocatalysts. *Nat. Mater.* **2013**, *12*, 81–87.

(8) Vidal-Iglesias, F. J.; Aran-Ais, R. M.; Solla-Gullon, J.; Herrero, E.; Feliu, J. M. Electrochemical Characterization of Shape-Controlled Pt Nanoparticles in Different Supporting Electrolytes. *ACS Catal.* **2012**, *2*, 901–910.

(9) Dsoke, S.; Kolary-Zurowska, A.; Zurowski, A.; Mignini, P.; Kulesza, P. J.; Marassi, R. Rotating Disk Electrode Study of CS3.5H0.5PW12O40 as Mesoporous Support for Pt Nanoparticles for PEM Fuel Cells Electrodes. *J. Power Sources* **2011**, *196*, 10591–10600.

(10) Poh, C. K.; Lim, S. H.; Tian, Z. Q.; Lai, L. F.; Feng, Y. P.; Shen, Z. X.; Lin, J. Y. Pt-WxC Nano-Composites as an Efficient Electrochemical Catalyst for Oxygen Reduction Reaction. *Nano Energy* **2013**, *2*, 28–39.

(11) Xiao, Y. P.; Jiang, W. J.; Wan, S.; Zhang, X.; Hu, J. S.; Wei, Z. D.; Wan, L. J. Self-Deposition of Pt Nanocrystals on Mn3O4 Coated Carbon Nanotubes for Enhanced Oxygen Reduction Electrocatalysis. *J. Mater. Chem. A* **2013**, *1*, 7463–7468.

(12) Zhu, Q.; Zhou, S. H.; Wang, X. Q.; Dai, S. Controlled Synthesis of Mesoporous Carbon Modified by Tungsten Carbides as an Improved Electrocatalyst Support for the Oxygen Reduction Reaction. *J. Power Sources* **2009**, *193*, 495–500.

(13) Liang, C. H.; Ding, L.; Li, C. A.; Pang, M.; Su, D. S.; Li, W. Z.; Wang, Y. M. Nanostructured WCx/CNTs as Highly Efficient Support of Electrocatalysts with Low Pt Loading for Oxygen Reduction Reaction. *Energy Environ. Sci.* **2010**, *3*, 1121–1127.

(14) Chen, G. Y.; Bare, S. R.; Mallouk, T. E. Development of Supported Bifunctional Electrocatalysts for Unitized Regenerative Fuel Cells. *J. Electrochem. Soc.* **2002**, *149*, A1092–A1099.

(15) Chhina, H.; Campbell, S.; Kesler, O. An Oxidation-Resistant Indium Tin Oxide Catalyst Support for Proton Exchange Membrane Fuel Cells. *J. Power Sources* **2006**, *161*, 893–900.

(16) Palaniselvam, T.; Irshad, A.; Unni, B.; Kurungot, S. Activity Modulated Low Platium Content Oxygen Reduction Electrocatalysts Prepared by Inducing Nano-Order Dislocations on Carbon Nanofiber through N-2-Doping. *J. Phys. Chem. C* **2012**, *116*, 14754–14763.

(17) Vogel, W.; Timperman, L.; Alonso-Vante, N. Probing Metal Substrate Interaction of Pt Nanoparticles: Structural XRD Analysis and Oxygen Reduction Reaction. *Appl. Catal., A* **2010**, *377*, 167–173.

(18) Timperman, L.; Feng, Y. J.; Vogel, W.; Alonso-Vante, N. Substrate Effect on Oxygen Reduction Electrocatalysis. *Electrochim. Acta* **2010**, *55*, 7558–7563.

(19) Liu, X.; Yao, K. X.; Meng, C. G.; Han, Y. Graphene Substrate-Mediated Catalytic Performance Enhancement of Ru Nanoparticles: A First-Principles Study. *Dalton Trans.* **2012**, *41*, 1289–1296.

(20) Li, Y.; Zhao, Y.; Cheng, H. H.; Hu, Y.; Shi, G. Q.; Dai, L. M.; Qu, L. T. Nitrogen-Doped Graphene Quantum Dots with Oxygen-Rich Functional Groups. *J. Am. Chem. Soc.* **2012**, *134*, 15–18.

(21) Zhang, Z. P.; Zhang, J.; Chen, N.; Qu, L. T. Graphene Quantum Dots: An Emerging Material for Energy-Related Applications and Beyond. *Energy Environ. Sci.* **2012**, *5*, 8869–8890.

(22) Tan, Y. M.; Xu, C. F.; Chen, G. X.; Zheng, N. F.; Xie, Q. J. A Graphene-Platinum Nanoparticles-Ionic Liquid Composite Catalyst for Methanol-Tolerant Oxygen Reduction Reaction. *Energy Environ. Sci.* **2012**, *5*, 6923–6927.

(23) Vinayan, B. P.; Nagar, R.; Ramaprabhu, S. Synthesis and Investigation of Mechanism of Platinum-Graphene Electrocatalysts by Novel Co-Reduction Techniques for Proton Exchange Membrane Fuel Cell Applications. *J. Mater. Chem.* **2012**, *22*, 25325–25334.

(24) Li, Y. J.; Li, Y. J.; Zhu, E. B.; McLouth, T.; Chiu, C. Y.; Huang, X. Q.; Huang, Y. Stabilization of High-Performance Oxygen Reduction Reaction Pt Electrocatalyst Supported on Reduced Graphene Oxide/Carbon Black Composite. *J. Am. Chem. Soc.* **2012**, *134*, 12326–12329.

(25) Seo, M. H.; Choi, S. M.; Kim, H. J.; Kim, W. B. The Graphene-Supported Pd and Pt Catalysts for Highly Active Oxygen Reduction Reaction in an Alkaline Condition. *Electrochem. Commun.* **2011**, *13*, 182–185.

(26) Li, Y.; Hu, Y.; Zhao, Y.; Shi, G. Q.; Deng, L. E.; Hou, Y. B.; Qu, L. T. An Electrochemical Avenue to Green-Luminescent Graphene Quantum Dots as Potential Electron-Acceptors for Photovoltaics. *Adv. Mater.* **2011**, *23*, 776–+.

(27) He, D. P.; Cheng, K.; Peng, T.; Sun, X. L.; Pan, M.; Mu, S. C. Bifunctional Effect of Reduced Graphene Oxides to Support Active Metal Nanoparticles for Oxygen Reduction Reaction and Stability. *J. Mater. Chem.* **2012**, *22*, 21298–21304.

(28) Park, S.; Ruoff, R. S. Chemical Methods for the Production of Graphenes. *Nat. Nanotechnol* **2009**, *4*, 217–224.

(29) Wu, Z. X.; Lv, Y. Y.; Xia, Y. Y.; Webley, P. A.; Zhao, D. Y. Ordered Mesoporous Platinum@Graphitic Carbon Embedded Nano-

phase as a Highly Active, Stable, and Methanol-Tolerant Oxygen Reduction Electrocatalyst. *J. Am. Chem. Soc.* **2012**, *134*, 2236−2245.
(30) Li, L.; Xing, Y. C. Electrochemical Durability of Carbon Nanotubes in Noncatalyzed and Catalyzed Oxidations. *J. Electrochem. Soc.* **2006**, *153*, A1823−A1828.
(31) Wang, J. J.; Yin, G. P.; Shao, Y. Y.; Wang, Z. B.; Gao, Y. Z. Investigation of Further Improvement of Platinum Catalyst Durability with Highly Graphitized Carbon Nanotubes Support. *J. Phys. Chem. C* **2008**, *112*, 5784−5789.
(32) Lim, D. H.; Wilcox, J. Mechanisms of the Oxygen Reduction Reaction on Defective Graphene-Supported Pt Nanoparticles from First-Principles. *J. Phys. Chem. C* **2012**, *116*, 3653−3660.
(33) He, D. P.; Kou, Z.; Xiong, Y.; Cheng, K.; Chen, X.; Pan, M.; Mu, S. Simultaneous Sulfonation and Reduction of Graphene Oxide as Highly Efficient Supports for Metal Nanocatalysts. *Carbon* **2014**, *66*, 312−319.
(34) He, G.; Song, Y.; Liu, K.; Walter, A.; Chen, S.; Chen, S. W. Oxygen Reduction Catalyzed by Platinum Nanoparticles Supported on Graphene Quantum Dots. *ACS Catal.* **2013**, *3*, 831−838.
(35) Tian, L.; Song, Y.; Chang, X. J.; Chen, S. W. Hydrothermally Enhanced Photoluminescence of Carbon Nanoparticles. *Scr. Mater.* **2010**, *62*, 883−886.
(36) Zhou, Y.; Bao, Q.; Tang, L. A. L.; Zhong, Y.; Loh, K. P. Hydrothermal Dehydration for the "Green" Reduction of Exfoliated Graphene Oxide to Graphene and Demonstration of Tunable Optical Limiting Properties. *Chem. Mater.* **2009**, *21*, 2950−2956.
(37) Pei, S. F.; Cheng, H. M. The Reduction of Graphene Oxide. *Carbon* **2012**, *50*, 3210−3228.
(38) Peng, J.; Gao, W.; Gupta, B. K.; Liu, Z.; Romero-Aburto, R.; Ge, L. H.; Song, L.; Alemany, L. B.; Zhan, X. B.; Gao, G. H.; Vithayathil, S. A.; Kaipparettu, B. A.; Marti, A. A.; Hayashi, T.; Zhu, J. J.; Ajayan, P. M. Graphene Quantum Dots Derived from Carbon Fibers. *Nano Lett.* **2012**, *12*, 844−849.
(39) Zhou, Z. Y.; Kang, X. W.; Song, Y.; Chen, S. W. Enhancement of the Electrocatalytic Activity of Pt Nanoparticles in Oxygen Reduction by Chlorophenyl Functionalization. *Chem. Commun.* **2012**, *48*, 3391−3393.
(40) Gloaguen, F.; Andolfatto, F.; Durand, R.; Ozil, P. Kinetic Study of Electrochemical Reactions at Catalyst-Recast Ionomer Interfaces from Thin Active Layer Modelling. *J. Appl. Electrochem.* **1994**, *24*, 863−869.
(41) Hull, R. V.; Li, L.; Xing, Y. C.; Chusuei, C. C. Pt Nanoparticle Binding on Functionalized Multiwalled Carbon Nanotubes. *Chem. Mater.* **2006**, *18*, 1780−1788.
(42) Chen, S. W.; Templeton, A. C.; Murray, R. W. Monolayer-Protected Cluster Growth Dynamics. *Langmuir* **2000**, *16*, 3543−3548.
(43) Wu, H.; Zhao, W.; Hu, H.; Chen, G. One-Step in situ Ball Milling Synthesis of Polymer-Functionalized Graphene Nanocomposites. *J. Mater. Chem.* **2011**, *21*, 8626−8632.
(44) Cui, L.; Liu, Z.; Duan, S.; Wu, D. Y.; Ren, B.; Tian, Z. Q.; Zou, S. Z. Orientation Change of Adsorbed Pyrazine on Roughened Rhodium Electrodes as Probed by Surface-Enhanced Raman Spectroscopy. *J. Phys. Chem. B* **2005**, *109*, 17597−17602.
(45) Ferrari, A. C.; Basko, D. M. Raman Spectroscopy as a Versatile Tool for Studying the Properties of Graphene. *Nat. Nanotechnol* **2013**, *8*, 235−246.
(46) Dresselhaus, M. S.; Terrones, M. Carbon-Based Nanomaterials from a Historical Perspective. *Proc. IEEE* **2013**, *101*, 1522−1535.
(47) Tuinstra, F.; Koenig, J. L. Raman Spectrum of Graphite. *J. Chem. Phys.* **1970**, *53*, 1126−1130.
(48) Ferrari, A. C. Raman Spectroscopy of Graphene and Graphite: Disorder, Electron-Phonon Coupling, Doping and Nonadiabatic Effects. *Solid State Commun.* **2007**, *143*, 47−57.
(49) Paredes, J. I.; Villar-Rodil, S.; Solis-Fernandez, P.; Martinez-Alonso, A.; Tascon, J. M. D. Atomic Force and Scanning Tunneling Microscopy Imaging of Graphene Nanosheets Derived from Graphite Oxide. *Langmuir* **2009**, *25*, 5957−5968.
(50) Rybachuk, M.; Bell, J. M. Electronic States of Trans-Polyacetylene, Poly(p-Phenylene Vinylene) and sp-Hybridised Carbon Species in Amorphous Hydrogenated Carbon Probed by Resonant Raman Scattering. *Carbon* **2009**, *47*, 2481−2490.
(51) Turgeon, S.; Paynter, R. W. On the Determination of Carbon sp(2)/sp(3) Ratios in Polystyrene-Polyethylene Copolymers by Photoelectron Spectroscopy. *Thin Solid Films* **2001**, *394*, 44−48.
(52) Dettlaff-Weglikowska, U.; Benoit, J. M.; Chiu, P. W.; Graupner, R.; Lebedkin, S.; Roth, S. Chemical Functionalization of Single Walled Carbon Nanotubes. *Curr. Appl. Phys.* **2002**, *2*, 497−501.
(53) Iucci, G.; Carravetta, V.; Altamura, P.; Russo, M. V.; Paolucci, G.; Goldoni, A.; Polzonetti, G. XPS, NEXAFS and Theoretical Study of Phenylacetylene Adsorbed on Cu(100). *Chem. Phys.* **2004**, *302*, 43−52.
(54) Siegbahn, K. Electron Spectroscopy for Chemical Analysis (Esca). *Philos. Trans. R. Soc., A* **1970**, *268*, 33−57.
(55) Zhang, S.; Chandra, K. L.; Gorman, C. B. Self-assembled Monolayers of Terminal Alkynes on Gold. *J. Am. Chem. Soc.* **2007**, *129*, 4876−4877.
(56) Bajpai, R.; Roy, S.; Kulshrestha, N.; Rafiee, J.; Koratkar, N.; Misra, D. S. Graphene Supported Nickel Nanoparticle as a Viable Replacement for Platinum in Dye Sensitized Solar Cells. *Nanoscale* **2012**, *4*, 926−930.
(57) Moon, I. K.; Lee, J.; Ruoff, R. S.; Lee, H. Reduced Graphene Oxide by Chemical Graphitization. *Nat. Commun.* **2010**, *1*, 73.
(58) Wagner, C. D.; Riggs, W. M.; Davis, L. E.; Moulder, J. F.; Muilenberg, G. E. *Handbook of X-Ray Photoelectron Spectroscopy: A Reference Book of Standard Data for Use in X-Ray Photoelectron Spectroscopy*; Perkin-Elmer Corp.: Eden Prairie, MN, 1979.
(59) Dablemont, C.; Lang, P.; Mangeney, C.; Piquemal, J. Y.; Petkov, V.; Herbst, F.; Viau, G. FTIR and XPS Study of Pt Nanoparticle Functionalization and Interaction with Alumina. *Langmuir* **2008**, *24*, 5832−5841.
(60) Lefevre, M.; Dodelet, J. P. Fe-Based Catalysts for the Reduction of Oxygen in Polymer Electrolyte Membrane Fuel Cell Conditions: Determination of the Amount of Peroxide Released during Electroreduction and Its Influence on the Stability of the Catalysts. *Electrochim. Acta* **2003**, *48*, 2749−2760.
(61) Gojkovic, S. L.; Gupta, S.; Savinell, R. F. Heat-Treated Iron(III) Tetramethoxyphenyl Porphyrin Chloride Supported on High-Area Carbon as an Electrocatalyst for Oxygen Reduction: Part III. Detection of Hydrogen-Peroxide during Oxygen Reduction. *Electrochim. Acta* **1999**, *45*, 889−897.
(62) Schumpe, A.; Adler, I.; Deckwer, W. D. Solubility of Oxygen in Electrolyte-Solutions. *Biotechnol. Bioeng.* **1978**, *20*, 145−150.
(63) Anastasijevic, N. A.; Dimitrijevic, Z. M.; Adzic, R. R. Oxygen Reduction on a Ruthenium Electrode in Acid Electrolytes. *Electrochim. Acta* **1986**, *31*, 1125−1130.
(64) Markovic, N. M.; Gasteiger, H. A.; Grgur, B. N.; Ross, P. N. Oxygen Reduction Reaction on Pt(111): Effects of Bromide. *J. Electroanal. Chem.* **1999**, *467*, 157−163.
(65) Jackson, A.; Viswanathan, V.; Forman, A. J.; Larsen, A. H.; Nørskov, J. K.; Jaramillo, T. F. Climbing the Activity Volcano: Core-Shell Ru@Pt Electrocatalysts for Oxygen Reduction. *ChemElectroChem* **2014**, *1*, 67−71.
(66) Chou, S.-W.; Lai, Y.-R.; Yang, Y. Y.; Tang, C.-Y.; Hayashi, M.; Chen, H.-C.; Chen, H.-L.; Chou, P.-T. Uniform Size and Composition Tuning of PtNi Octahedra for Systematic Studies of Oxygen Reduction Reactions. *J. Catal.* **2014**, *309*, 343−350.
(67) Lim, B.; Jiang, M. J.; Camargo, P. H. C.; Cho, E. C.; Tao, J.; Lu, X. M.; Zhu, Y. M.; Xia, Y. N. Pd-Pt Bimetallic Nanodendrites with High Activity for Oxygen Reduction. *Science* **2009**, *324*, 1302−1305.
(68) Yeo, K. M.; Choi, S.; Anisur, R. M.; Kim, J.; Lee, I. S. Surfactant-Free Platinum-on-Gold Nanodendrites with Enhanced Catalytic Performance for Oxygen Reduction. *Angew. Chem., Int. Ed.* **2011**, *50*, 745−748.
(69) Liu, L. F.; Pippel, E. Low-Platinum-Content Quaternary PtCuCoNi Nanotubes with Markedly Enhanced Oxygen Reduction Activity. *Angew. Chem., Int. Ed.* **2011**, *50*, 2729−2733.
(70) Norskov, J. K.; Rossmeisl, J.; Logadottir, A.; Lindqvist, L.; Kitchin, J. R.; Bligaard, T.; Jonsson, H. Origin of the Overpotential for

Oxygen Reduction at A Fuel-Cell Cathode. *J. Phys. Chem. B* **2004**, *108*, 17886−17892.
(71) Stephens, I. E. L.; Bondarenko, A. S.; Perez-Alonso, F. J.; Calle-Vallejo, F.; Bech, L.; Johansson, T. P.; Jepsen, A. K.; Frydendal, R.; Knudsen, B. P.; Rossmeisl, J.; Chorkendorff, I. Tuning the Activity of Pt(111) for Oxygen Electroreduction by Subsurface Alloying. *J. Am. Chem. Soc.* **2011**, *133*, 5485−5491.
(72) Stephens, I. E. L.; Bondarenko, A. S.; Gronbjerg, U.; Rossmeisl, J.; Chorkendorff, I. Understanding the Electrocatalysis of Oxygen Reduction on Platinum and its Alloys. *Energy Environ. Sci.* **2012**, *5*, 6744−6762.